Frontiers in Bioscience Landmark

Front. Biosci. (Landmark Ed) **2025**; 30(5): 36781
https://doi.org/10.31083/FBL36781

Original Research

Mechanism of *SLC1A5* Regulation of Glutamine Metabolism to Promote Ferroptosis Sensitivity in Endometriosis

Hui-Yu Ma[1], Huan-Yu Wu[1], Yu-Ting Xiang[1], Yu-Yin Liu[1], Jin Xie[1], Peng-Yu Cai[1], Bin Zhang[1], Yu-Hang Zhang[1], Ming-Xiu Wu[1,*]

[1]Department of Obstetrics and Gynecology, The Tenth Affiliated Hospital, Southern Medical University (Dongguan People's Hospital), 523058 Dongguan, Guangdong, China

*Correspondence: wmx751010@126.com (Ming-Xiu Wu)

Academic Editor: Yongmei Xi

Submitted: 5 January 2025 Revised: 31 March 2025 Accepted: 25 April 2025 Published: 21 May 2025

Abstract

Background: Endometriosis (EMs) is a chronic gynecological disorder associated with ectopic endometrial tissue, inflammation, oxidative stress, and mitochondrial dysfunction. A promising strategy for treating EMs is to target ferroptosis, a programmed cell death mechanism regulated by reactive oxygen species (ROS) and glutamine metabolism. Solute carrier family 1 member 5 (*SLC1A5*), a glutamine transporter, and *c-Myc* play key roles in ferroptosis, forming a "ROS/*c-Myc*/*SLC1A5*" feedback loop. The aim of this study was to investigate the regulatory role of *SLC1A5* in ferroptosis. In addition, we evaluated the ferroptosis inducer Erastin as a potential therapeutic agent for EMs. **Methods**: The human endometrial stromal cells (ESCs) line hEM15A was used in this study, together with a rat model of EMs. hEM15A cells and rats were treated with Erastin, with or without *SLC1A5* modulation or ROS scavenging with N-acetylcysteine (NAC). Cell viability, ROS levels, glutamine metabolism, mitochondrial function, and ferroptosis markers (glutathione peroxidase 4 (GPX4)) were subsequently analyzed by Cell Counting Kit-8 (CCK-8) assay, reverse transcription quantitative polymerase chain reaction (RT-qPCR), Western blot, and fluorescent probes. Pathological changes, lesion volumes, and pelvic adhesions in the rat EM model were assessed using hematoxylin and eosin (HE) staining, ultrasound imaging, and Haber scoring. **Results**: Erastin treatment of ESCs induced ferroptosis by upregulating *SLC1A5* and *c-Myc* expression, increasing ROS levels, and altering glutamine metabolism. Overexpression of *SLC1A5* enhanced sensitivity to ferroptosis, whereas *SLC1A5* knockdown and NAC treatment reversed these effects. Mechanistically, *c-Myc* bound to the *SLC1A5* promoter, forming positive feedback with ROS. In the rat model of EMs, Erastin treatment reduced ectopic lesion volume, pelvic adhesions, and inflammatory markers (TNF-α, IL-6, IL-1β). These therapeutic effects were mitigated by NAC, highlighting the importance of the ROS/*c-Myc*/*SLC1A5* pathway. **Conclusions**: This study confirmed the involvement of the ROS/*c-Myc*/*SLC1A5* pathway in regulating EMs sensitivity to ferroptosis and demonstrated the potential of Erastin as a therapeutic agent. Targeting this pathway offers a promising approach for the treatment of EMs.

Keywords: endometriosis (EMs); *SLC1A5*; glutamine metabolism; ferroptosis; reactive oxygen species (ROS)

1. Introduction

Endometriosis (EMs) is characterized by the presence of endometrial tissue outside the uterine cavity, commonly in the ovaries, fallopian tubes and pelvis [1]. This chronic gynecological disorder is associated with pelvic inflammation and oxidative stress, and is a major contributor to menstrual pain, reduced fertility, and persistent pelvic discomfort [2]. Based on the site of occurrence, EMs is primarily classified into ovarian, peritoneal, and deep infiltrating types [3]. The incidence of endometriosis is on the rise [4]. The clinical management of EMs typically involves surgical and pharmacological interventions. Laparoscopic surgery inevitably impairs the ovarian reserve and is associated with a risk of recurrence, while long-term pharmacological treatments, such as Gonadotropin-Releasing Hormone Agonist (GNRH-a) and progesterone, are often linked to significant side effects [5]. Consequently, there is a pressing need for safer and more effective medications to treat EMs, with reduced adverse effects [6].

The endometrial stromal cells (ESCs) in patients with EMs exhibit abnormally increased proliferation and migration capacities [7,8]. Dysfunctional mitochondrial metabolism in these cells increases energy production, thereby encouraging the growth of ectopic endometrial tissue and exacerbating disease progression in EMs [9,10]. Ferroptosis is a recently identified form of programmed cell death that is regulated by various factors, including reactive oxygen species (ROS) [11,12]. Triggering of ferroptosis curbs the growth of endometrial tissue, suggesting that its modulation could be an effective strategy for managing EMs [13]. Solute carrier family 1 member 5 (*SLC1A5*) has been identified as a key regulator in the ferroptosis pathway, potentially through its role in glutamine (Gln) metabolism. Additionally, *c-Myc* transcriptional activity is regulated by ROS, while *c-Myc*, in turn, promotes the transcriptional activation of *SLC1A5* [14–16]. This suggests potential interactions between ROS, *c-Myc*, and *SLC1A5* in the pathogenesis of EMs. In the present study, we hypothesized that

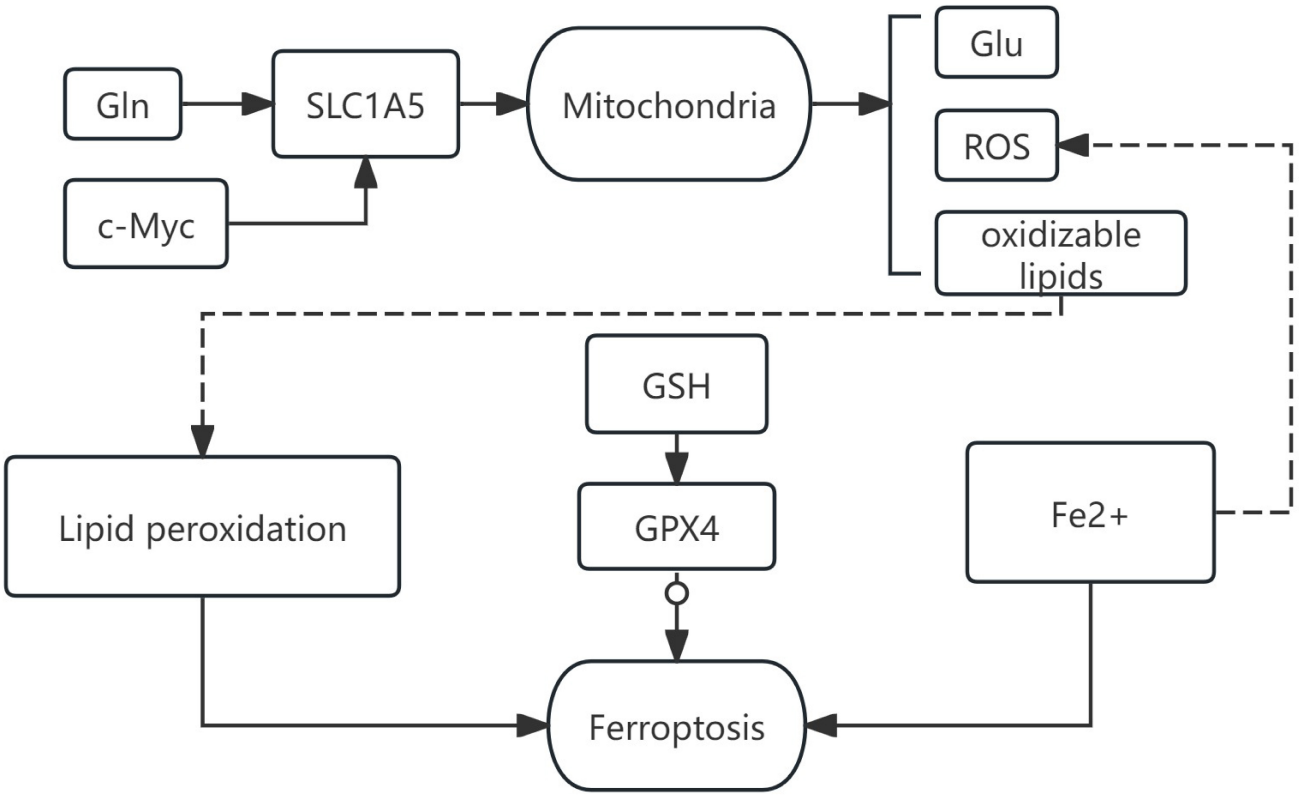

Fig. 1. This figure shows the research content and hypotheses of this paper. Gln, glutamine; *SLC1A5*, Solute carrier family 1 member 5; Glu, glutamate; ROS, reactive oxygen species; GSH, Glutathione; GPX4, glutathione peroxidase 4.

SLC1A5 might be a viable treatment target for ectopic sites of EMs because of its role in Erastin-triggered ferroptosis (Fig. 1).

This study revealed active involvement of *SLC1A5*, *c-Myc*, and Gln in the pathogenies of EMs. Erastin was found to regulate *SLC1A5*, *c-Myc*, Gln, and oxidative stress in ESCs and in a rat EMs model, thereby enhancing sensitivity to ferroptosis. Furthermore, Erastin significantly reduced the ectopic EMs lesion volume and pelvic adhesions in a rat model, underscoring its potential as a therapeutic agent. These findings suggest that Erastin may be a promising treatment for EMs through its modulation of the ROS/*c-Myc*/*SLC1A5* pathway.

2. Materials and Methods

2.1 Cell Culture and Treatment Interventions

The immortalized cell line hEM15A provides a consistent and reproducible experimental system, allowing repeated experiments without the variability or limited lifespan inherent to primary cells. This reproducibility makes it an ideal model for studying EMs-related mechanisms, such as sensitivity to ferroptosis. In this study, the human ESCs line hEM15A (PN-H156A, Wuhan Punosei Life Technology, Wuhan, China) was cultured in a complete medium specifically formulated for hEM15A. Cells were maintained under standard conditions in a CO_2 incubator at 37 °C with 5% CO_2. When the cells in a T25 flask reached 90% confluency, the spent medium was removed and cells were washed twice with 2 mL of phosphate-buffered saline (PBS; PN-SH30256.01, Hyclone, Logan, UT, USA). After removing the PBS, 1 mL of 0.25% trypsin (PN-25200056, Gibco, Shanghai, China) was added and the cells examined through a microscope (Thermo Fisher, Hillsboro, OR, USA) for 1–3 minutes until they became rounded in shape. To neutralize the trypsin, 5 mL of complete culture medium (PN-CPM-HES5, Procell, Wuhan, China) was added and the cells were gently pipetted to ensure proper collection.

The cell mixture was spun at 800 rpm for 5 minutes at 4 °C and the medium was then removed. The cell pellet was resuspended in complete culture medium and transferred to culture flasks, with the medium replaced every other day. For cryopreservation, the cells were frozen in a mixture consisting of 95% complete culture medium and 5% DMSO (PN-CPS-HESD5, Procell, China) and stored in liquid nitrogen. Each experiment utilized cells during the exponential growth stage. The cell line was validated by short tandem repeat (STR) profiling and tested negative for mycoplasma.

For the Erastin group, hEM15A cells were treated with 20 µmol/L of the ferroptosis inducer Erastin (S7242, Selleck, Houston, TX, USA) for 24 h. The overexpression (OE)-*SLC1A5*+Erastin and OE-negative control (NC)+Erastin groups were generated by transfecting

Table 1. RT-qPCR primers.

Gene	Forward primer sequence	Reverse primer sequence
SLC1A5	5′-CCAACTCAAGGCTAGAAAACAG-3′	5′-AGGTATTTGTCCTCAGCCTC-3′
c-Myc	5′-CCTGGTGCTCCATGAGGAGA-3′	5′-GCTCTTGGAGCAGCTTCACA-3′
GAPDH	5′-GGTCTCCTCTGACTTCAACA-3′	5′-GTGAGGGTCTCTCTCTTCCT-3′

RT-qPCR, reverse transcription quantitative polymerase chain reaction.

Erastin group cells with *SLC1A5* OE adenovirus vector (G31424, GenePharma, Shanghai, China) and an empty (NC) vector (GenePharma, G00000), respectively. Similarly, transfection of the Erastin group with *SLC1A5* knockdown (KD) vector (GenePharma, G31425) or an empty (NC) vector (GenePharma, G00000) created the KD-*SLC1A5*+Erastin and KD-NC+Erastin groups, which used siRNA. The siRNA sequences were as follows: Sense strand: 5′-GUCGACCAUAUCUCCUUGAdTdT-3′; Antisense strands: 5′-UCAAGGAGAUAUGGUCGACdTdT-3′. The negative control siRNA (si-NC), which does not target any human gene, was also provided by GenePharma with the following sequences: Sense strand: 5′-UUCUCCGAACGUGUCACGUdTdT-3′; Antisense strand: 5′-ACGUGACACGUUCGGAGAAdTdT-3′. The Erastin+N-acetylcysteine (NAC) group was established by treating Erastin group cells with 5 mmol/L NAC, a ROS scavenger (Beyotime, Shanghai, China, S0077), for 24 h [17].

2.2 CCK-8 Assay

hEM15A cells undergoing exponential growth were placed into 96-well plates at 5×10^3 cells per well and grown in a 5% CO_2 environment at 37 °C for 24 h. The culture medium in each well was then replaced with fresh medium containing 20 µM Erastin and incubated for an additional 24 h. Following this, 10 µL of Cell Counting Kit-8 (CCK-8) solution was added to each well containing 100 µL of cell culture medium, and the cells incubated for 2 h. Absorbance at 450 nm was then measured using a microplate reader (Thermo Fisher, USA) [18].

2.3 Analysis of ROS and MDA

hEM15A cells treated with Erastin were washed with 1 mL of PBS. A 200 nM working solution of Mito-Tracker Red CMXRos (mitochondrial ROS red fluorescent probe, Beyotime, China, C1035) was prepared. The cells were incubated with 1 mL of the working solution at 37 °C in a 5% CO_2 incubator for 30 minutes, followed by three washes with PBS. Fluorescence was observed under a fluorescence microscope (Thermo Fisher, USA) within 2 h of staining.

Cell culture supernatants from each group were collected and analyzed using the human Malondialdehyde (MDA) ELISA Kit (Hnybio, Shanghai, China, HNY-E1035) according to the manufacturer's instructions. Light absorption at 450 nm was measured with an RT-6000 plate reader (RT-6000, Rayto, Shenzhen, China) [19].

2.4 RNA Extraction, cDNA Synthesis, and qPCR

Total cellular RNA was extracted using Trizol reagent (9109, Takara Bio, Shiga, Japan) and purified by chloroform phase separation, isopropanol precipitation, and washing with 75% ethanol. The RNA concentration and purity were assessed with a NanoDrop 2000 device (Thermo Fisher Scientific, USA, ND-2000) by measuring the 260/280 absorbance ratio. A ratio between 1.9 and 2.1 was considered to indicate satisfactory purity.

The purified RNA was reverse transcribed into cDNA using the HiScript III First Strand cDNA Synthesis Kit (R312-01, Vazyme, Nanjing, China). The reverse transcription reaction was carried out by incubating at 25 °C for 5 minutes, 42 °C for 30 minutes, and 85 °C for 5 minutes. Quantitative real-time PCR (qPCR) was then conducted with the CFX96 Touch system (1855195, Bio-Rad, Hercules, CA, USA).

The qPCR process involved initial heating at 95 °C for 30 seconds, followed by 40 cycles of melting at 95 °C for 10 seconds, binding at 60 °C for 30 seconds, and lengthening at 72 °C for 15 seconds. Melting curve analysis was performed by holding at 60 °C for 60 seconds, then heating to 95 °C for 15 seconds. Experimental results were calculated using the $2^{-\Delta\Delta Ct}$ method [20]. Specific primers for PCR amplification were synthesized based on the sequences listed in Table 1.

2.5 Western Blot

Cells were washed three times with ice-cold PBS and lysed on ice for 30 min in RIPA buffer (Beyotime, China, P0013B) containing PMSF (Beyotime, ST506) and a cocktail of protease inhibitors (P8340, Sigma, Burlington, MA, USA). Lysates were centrifuged at 12,000 rpm for 15 min at 4 °C, and the supernatants collected. Protein concentrations were measured using the Enhanced BCA Protein Assay Kit (Beyotime, P0010), and 40 µg aliquots were stored at –80 °C. Samples were mixed with sodium dodecyl sulfate polyacrylamide gel electrophoresis (SDS-PAGE) loading buffer (Beyotime, P0015L), boiled at 95 °C for 10 min, separated on 10% SDS-PAGE gels, and transferred to 0.45 µm Polyvinylidene Fluoride (PVDF) membrane. Membranes were blocked with 5% nonfat milk in Tris-Buffered Saline with Tween 20 (TBST) for 1 h at room temperature, then incubated overnight at 4 °C with the following primary antibodies: anti-SLC1A5 (1:1000, Abcam, Cambridge, UK, ab237704), anti-c-Myc (1:1000, Abcam, UK, ab32072), and anti-GPX4 (1:1000, Abcam, UK, ab125066), and anti-

β-actin (1:5000, Abcam, UK, ab8227), and anti-GAPDH (1:5000, Abcam, UK, ab181602) as an internal reference for loading control. After three 15-min washes with TBST, membranes were incubated with Horseradish Peroxidase (HRP)-conjugated secondary antibodies (Bioss, Beijing, China, bs-0295G-HRP) or 1–2 h at room temperature. Protein bands were detected using an ECL kit (NCM Biotech, Suzhou, China, P10300), quantified with ImageJ (v1.5, National Institutes of Health, Bethesda, MD, USA), and normalized to GAPDH and β-actin [21].

2.6 Measurement of Glutamate, Glutamine, Glutathione, and Fe^{2+} Levels

The cell supernatant was collected and standard curves for Gln and glutamate (Glu) were generated using the Glutamine Assay Kit (Colorimetric, Abcam, UK, ab197011) and the Glutamate Assay Kit (Colorimetric, Abcam, UK, ab83389), respectively. For each measurement, 50 µL of either the standard or sample was pipetted into a 96-well plate. The reaction mix was prepared and added according to the respective kit instructions. The plates were then incubated at 37 °C for 30 minutes in the dark, and absorbance was measured at 450 nm using an enzyme labeling instrument (4376600, Thermo Fisher Scientific, Vantaa, Uusimaa, Finland) [22].

Cell culture supernatants from each group were analyzed using the human Glutathione (GSH) ELISA Kit (Hnybio, Shanghai, China, HNY-E1080) according to the manufacturer's instructions, with absorbance measured at 450 nm using the RT-6000 microplate reader (Rayto, China, RT-6000). The E-BC-K773-M Ferrous Ion Colorimetric Assay Kit (Elabscience Biotechnology, Wuhan, China, E-BC-K773-M) was used to evaluate ferrous ion (Fe^{2+}) content by measuring absorbance at 593 nm, as described in the kit instructions [22].

2.7 Mitochondrial Membrane Potential

To prepare the working solution for evaluation of mitochondrial membrane potential, 30 µL of JC-1 (200X, Beyotime, China, C2006) was added to 4.8 mL of dilution buffer, followed by the addition of 1.2 mL of JC-1 staining buffer (5×, Beyotime, China, C2006). One mL of the JC-1 staining working solution was then added to the hEM15A cell culture and incubated at 37 °C for 20 minutes. After incubation, the cells were washed with 1 mL of JC-1 staining buffer (1×, Beyotime, China, C2006) and observed under a fluorescence microscope (Thermo Fisher, USA) [23].

2.8 ChIP-PCR

To assess c-Myc binding to *SLC1A5*, cells were fixed with 1% formaldehyde (Beyotime, P0099) for 10 min, quenched with 0.125 M glycine (Sigma, G8898), and lysed in SDS buffer (Beyotime, P0013) with protease inhibitors (Beyotime, P2076). Chromatin was sheared by sonication and then centrifuged. The resulting supernatant was precleared by incubating with 900 µL ChIP Dilution Buffer, 20 µL 50× Protease Inhibitor Cocktail (PIC) (78430, Thermo Fisher Scientific, Waltham, MA, USA), and 60 µL Protein Agarose/Salmon Sperm DNA (Beyotime, P2076) for 1 h at 4 °C. After adding 1 µL of antibody, the samples were incubated overnight at 4 °C. Immune complexes were washed (Beyotime, P2076) and eluted with 100 µL 10% SDS, 100 µL 1 M $NaHCO_3$, and 800 µL ddH_2O. Cross-links were reversed at 65 °C overnight with 20 µL 5 M NaCl. DNA was purified by incubation with 10 µL 0.5 M EDTA, 20 µL 1 M Tris-HCl (pH 6.5), and 2 µL proteinase K (Beyotime, ST506) at 45 °C for 2 h, then analyzed by reverse transcription quantitative polymerase chain reaction (RT-qPCR) [24].

2.9 Rat Model of EMs

The estrogen-driven reproductive cycle in rats aligns with the hormonal basis of human EMs, making it a relevant system for studying lesion dynamics and therapeutic responses. To establish the rat EMs model, specific pathogen free (SPF)-grade SD rats weighing 160–200 g aged 6–8 weeks were purchased from the Laboratory Animal Co., Ltd. (Guangzhou, Guangdong, China). The animals were housed at 20–25 °C with 40–70% humidity, a 10 h light cycle, and *ad libitum* access to food and water. After a one-week acclimation period, the rats were randomly assigned to the EMs model group (n = 15) and control group (sham surgery group) (n = 5). Daily oral administration of estradiol valerate (0.1 mg/kg, Sigma-Aldrich, USA, Cat#: E1631) for 3 days was used to synchronize the estrous cycle and stimulate endometrial proliferation. Following isoflurane anesthesia (3% induction and 1.5–2% maintenance, Lunan Better Pharmaceutical Co., Ltd., Guangzhou, China), the route of administration is inhalation, a 0.5 cm^2 piece of endometrial tissue from the left uterine horn was transplanted to the right abdominal wall in the EMs group. The sham surgery group underwent the same procedure but without endometrial tissue transplantation. Two weeks post-surgery, the abdominal tissues were harvested and hematoxylin and eosin (HE) histopathology was performed to confirm successful development of the EMs model. Rats were euthanized humanely in accordance with animal welfare guidelines using carbon dioxide (CO_2) inhalation followed by cervical dislocation.

Two weeks post-surgery, EMs model rats were treated daily with intraperitoneal Erastin (40 mg/kg) [25] alone (n = 5) or in combination with NAC (250 mg/kg) (n = 5) for 28 consecutive days to establish the respective treatment groups. The experimental protocols were approved by the Medical Ethics Review Board of The Tenth Affiliated Hospital, Southern Medical University (Dongguan People's Hospital) (Approval No. IACUC-AWEC-202410028) [26].

Table 2. RT-qPCR primers.

Gene	Forward primer sequence	Reverse primer sequence
SLC1A5	5′-GGATCTACACCACCTGAGCG-3′	5′-ACTGGGAGTTGAGAGAGCCT-3′
c-Myc	5′-TGCGATCCTGACGATGAGAC-3′	5′-GGTAAGAGGCCAGCTTCTCG-3′
GAPDH	5′-AGACAGCCGCATCTTCTTGT-3′	5′-ATCCGTTCACACCGACCTTC-3′

2.10 HE Staining and Analysis of ROS

Tissue samples were fixed, rinsed, and preserved in 70%–80% ethanol. They underwent graded ethanol dehydration and xylene clearing before paraffin infiltration and embedding. Sections (4 µm) were prepared, mounted on slides, and subjected to HE staining [27].

For the evaluation of ROS in tissue sections, DCFH-DA (Thermo Fisher Scientific, D6883) was diluted 1:1000 in serum-free medium to 10 µmol/L. Tissue sections were incubated with 200 µL of this solution at 37 °C for 30 min in a Thermo Fisher Heracell VIOS 160i incubator, allowing DCFH-DA to react with intracellular ROS. After three washes with PBS (Thermo Fisher, 10010023), ROS fluorescence was imaged using an Olympus (Guangzhou, Guangdong, China) IX83 microscope (excitation 488 nm, emission 525 nm) [28].

2.11 Measurement With Ultrasound Imaging and Haber Scoring Standard

The volume of abdominal ectopic EM lesions was measured using an ultrasound imaging system, followed by laparotomy under isoflurane anesthesia (3% induction, 1.5–2% maintenance) for lesion exposure. Pelvic adhesions were quantified on a scale from 0 (absent) to 10 (extensive), based on the degree of adhesion around the ectopic lesions and intestines. A score of 0 indicated no adhesions, while a score of 10 indicated severe adhesions involving the mesentery and peritoneum [29].

2.12 RT-qPCR for the Detection of SLC1A5 and c-Myc Expression in the Rat EM Model

To quantify *SLC1A5* and *c-Myc* expression in rat EM lesions, RT-qPCR was performed using the FastPure Tissue Total RNA Isolation Kit (Beyotime, China). Total RNA was extracted from 10 mg of fresh tissue with 500 µL Buffer RL, homogenized, and purified through FastPure RNA Columns III with sequential washes (700 µL Buffer RW1, 700 µL then 500 µL Buffer RW2 with ethanol). RNA was eluted with 30 µL RNase-free ddH_2O and quantified using a NanoDrop 2000 instrument (Thermo Fisher Scientific, USA). For cDNA synthesis, 500 ng RNA was reverse-transcribed in a 20 µL reaction volume (5× gDNA wiper mix, Hiscript III Enzyme Mix, Oligo(dT)20VN, Random hexamers) at 37 °C for 15 min and 85 °C for 5 s. RT-qPCR was conducted in a 20 µL system with 5 µL diluted cDNA, 2× Taq Pro Universal SYBR qPCR Master Mix, and specific primers (Table 2), using the CFX96 Touch system. The cycling conditions were: 95 °C for 30 s, followed by 40 cycles of 95 °C for 10 s, 60 °C for 30 s, and 95 °C for 15 s, with melt curve analysis from 65 °C to 95 °C. Expression was analyzed using the $2^{-\Delta\Delta Ct}$ method. Additional details can be found in the **Supplementary Material**.

2.13 Detection of Gln and Glu Levels in Rat EM Lesions

The Glutamine Assay Kit (Colorimetric) (ab197011) and Glutamate Assay Kit (ab83389) (Abcam, UK) were used to measure Gln and Glu, respectively. Approximately 0.1 g of tissue was blended with 1 mL of Reagent 1 provided in the assay kit in a chilled bath. The mixture was spun at 10,000 rpm for 10 minutes at 4 °C, and the upper liquid collected for further testing. Absorbance at 450 nm was measured using an RT-6000 microplate reader (Rayto, China, RT-6000) [30].

2.14 ELISA Detection of Serum TNF-α, IL-6, and IL-1β Levels

Blood was collected from the eyeball of rats and allowed to stand at room temperature for 30 minutes to 2 h, avoiding vigorous shaking to prevent hemolysis. Once the blood clotted naturally and the serum separated, the sample was centrifuged for 10 min at 4 °C and 2000 rpm. The supernatant was collected and placed on ice for later use. Standards were prepared by diluting in a 96-well plate according to the instructions provided in the ELISA kit manuals. The following ELISA kits were used: rat TNF-α ELISA Kit (PT516, Beyotime, China), rat IL-6 ELISA Kit (PI328, Beyotime, China), and rat IL-1β ELISA Kit (PI303, Beyotime, China). Light absorption at 450 nm was determined with a Rayto RT-6000 plate reader (China).

2.15 Statistical Analysis

Results were shown as the mean ± SD, and calculated and graphed with GraphPad Prism 9 (Dotmatics, Boston, MA, USA). The *t*-test was used to compare two groups, while one-way ANOVA examined differences across multiple groups. In cases of non-normal data, the Kruskal-Wallis test was applied, followed by Dunn's post hoc test. *p*-values below 0.05 indicated statistical significance: $*p < 0.05$, $**p < 0.01$, and $***p < 0.001$ [25].

3. Results

3.1 Erastin Increases Both ROS and Glutamine Metabolism, Potentially via Upregulation of SLC1A5

We first investigated the mechanism by which Erastin induces ferroptosis in hEM15A cells. The CCK-8 assay revealed that treatment with Erastin reduced the cell prolifera-

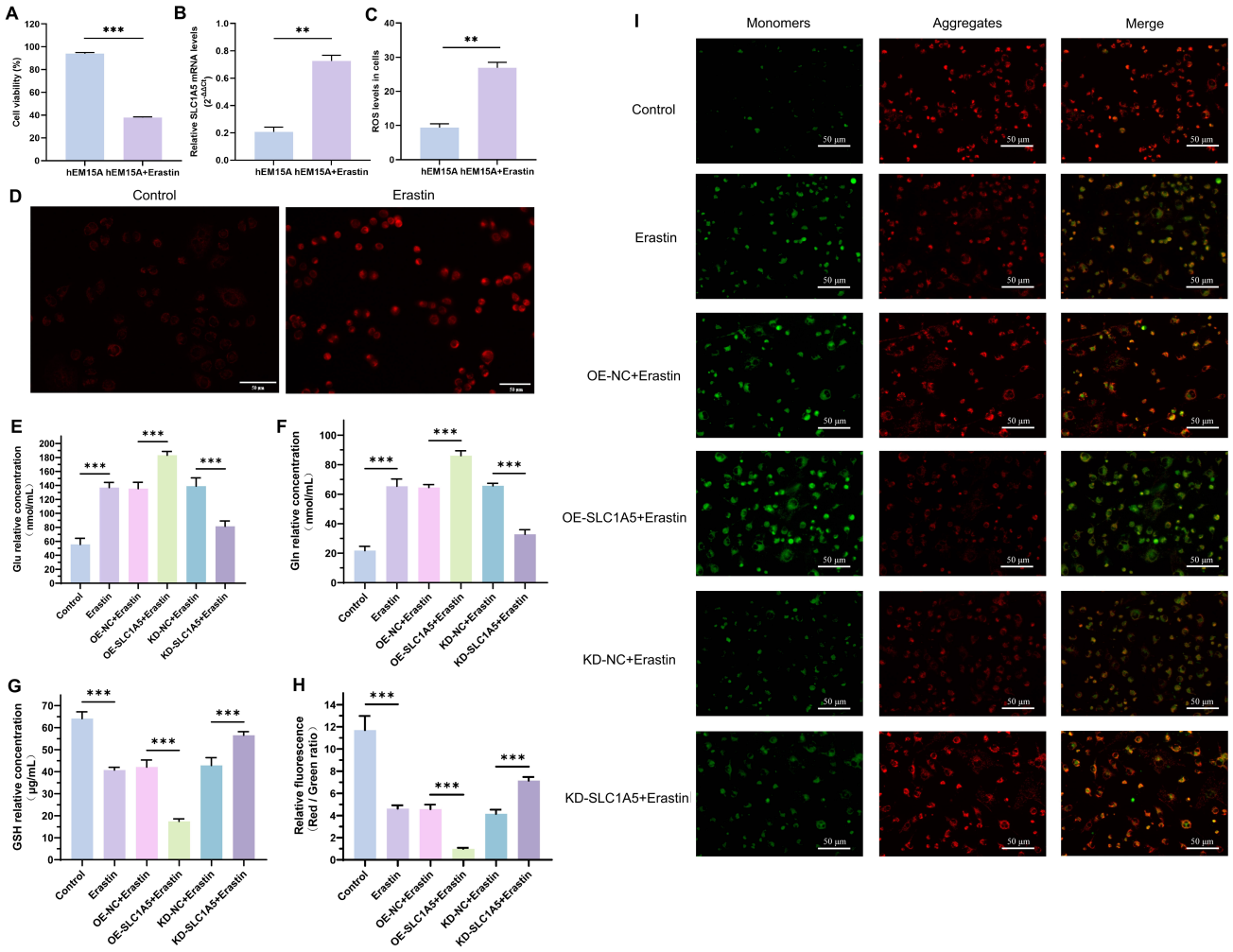

Fig. 2. Cellular responses, *SLC1A5* expression, and metabolic and mitochondrial functions of hEM15A cells under different treatment conditions, including Erastin treatment. (A) The Cell Counting Kit-8 (CCK-8) assay revealed reduced cell viability after treatment of hEM15A cells with Erastin, indicating induction of ferroptosis. (B) RT-qPCR showed that Erastin treatment increased the expression of *SLC1A5* mRNA. (C,D) Erastin treatment increased the reactive oxygen species (ROS) level in hEM15A cells, as indicated by the fluorescence intensity of ROS-specific probes (C1035). Scale bar: 50 µm. (E–G) Glu and Gln levels were significantly increased in hEM15A cells following Erastin treatment, with the overexpression (OE)-*SLC1A5*+Erastin group showing further upregulation and the knockdown (KD)-*SLC1A5*+Erastin group showing reduced levels ($p < 0.001$). Additionally, Erastin decreased the GSH level in hEM15A cells. Overexpression of *SLC1A5* also downregulated GSH, whereas *SLC1A5* knockdown increased GSH ($p < 0.001$). Experimental Groups: Control; Erastin; OE-*SLC1A5*+Erastin group, OE-*SLC1A5*: *SLC1A5* overexpression; OE-negative control (NC)+Erastin group, OE-NC: empty (NC) vector; KD-*SLC1A5*+Erastin group, KD-*SLC1A5*: *SLC1A5* KD; KD-NC+Erastin group, KD-NC: empty (NC) vector. (H,I) The mitochondrial membrane potential was evaluated using JC-1 dye, with results presented as histograms and fluorescent images. Erastin treatment decreased the mitochondrial membrane potential in hEM15A cells, with no change observed in empty vector-transfected cells. Overexpression of *SLC1A5* lowered the mitochondrial membrane potential, whereas *SLC1A5* knockdown increased the mitochondrial membrane potential, suggesting that Erastin regulates mitochondrial Gln metabolism via *SLC1A5*. Scale bar: 50 µm. $^{**}p < 0.01$, $^{***}p < 0.001$, n = 3.

tion rate (Fig. 2A), while RT-qPCR showed that it increased the expression of *SLC1A5* mRNA (Fig. 2B). Additionally, Erastin was observed to increase ROS levels in hEM15A cells, as indicated by ROS fluorescent probes (Fig. 2C,D). These findings suggest that Erastin increases ROS levels in hEM15A cells, possibly via upregulation of *SLC1A5*.

We next investigated the role of *SLC1A5* in Gln metabolism. The levels of Glu and Gln were significantly increased in hEM15A cells ($p < 0.001$) following Erastin treatment (Fig. 2E,F). Compared to the OE-NC+Erastin group, the OE-*SLC1A5*+Erastin group showed significantly upregulated levels of Glu and Gln ($p < 0.001$), while knock-

down of *SLC1A5* expression in the KD-*SLC1A5*+Erastin group reduced the levels of Glu and Gln ($p < 0.001$). Erastin also decreased the level of GSH in hEM15A cells ($p < 0.001$) (Fig. 2G). Overexpression of *SLC1A5* downregulated the GSH level, while knockdown of *SLC1A5* increased the level ($p < 0.001$). GSH is a primary cellular antioxidant that plays a critical role in protecting cells from oxidative stress by neutralizing ROS and supporting the function of glutathione peroxidase 4 (GPX4), a key enzyme that inhibits ferroptosis [11].

Erastin treatment decreased the mitochondrial membrane potential in hEM15A cells, but it remained unchanged in empty vector-transfected cells (Fig. 2H,I). Overexpression of *SLC1A5* lowered the mitochondrial membrane potential in hEM15A cells, whereas knockdown of *SLC1A5* raised the potential. These findings indicate that Erastin regulates mitochondrial Gln metabolism via *SLC1A5*.

3.2 SLC1A5 Regulates Ferroptosis via Glutamine Metabolism and Oxidative Stress

After modulating the expression of *SLC1A5*, ROS levels in each hEM15A cell group were assessed using ROS fluorescent probes. As shown in Fig. 3A,B, Following Erastin treatment, overexpression of *SLC1A5* increased the ROS levels in hEM15A cells, which was reversed upon *SLC1A5* knockdown ($p < 0.001$). As shown in Fig. 3C,D, Erastin significantly increased the levels of Fe^{2+} and MDA ($p < 0.001$). Overexpression of *SLC1A5* further enhanced the levels of Fe^{2+} and MDA, whereas knockdown of *SLC1A5* reduced these levels.

Western blot analysis was employed to assess the expression levels of c-Myc and the ferroptosis-related protein GPX4. The latter is a key regulator of ferroptosis and acts as a potent inhibitor, thus playing a critical role in its modulation [31]. Erastin induced *c-Myc* expression and inhibited GPX4 expression in hEM15A cells (Fig. 3E). After transfection with the *SLC1A5* overexpression plasmid, *c-Myc* expression increased significantly ($p < 0.001$), while GPX4 expression decreased ($p < 0.01$). Conversely, silencing of *SLC1A5* in hEM15A cells reduced *c-Myc* expression and increased GPX4 expression (both $p < 0.001$).

3.3 Erastin Enhances Sensitivity to Ferroptosis via the ROS/c-Myc/SLC1A5 Pathway

The above findings indicate that Erastin increases ROS, *c-Myc*, and *SLC1A5* expression. To explore the mechanism involved, the ROS scavenger NAC was used to intervene in Erastin-treated hEM15A cells. ChIP-PCR experiments revealed that *c-Myc* binds to the promoter region of *SLC1A5*, thereby increasing its transcription. *SLC1A5* mRNA expression was suppressed after ROS levels were reduced by NAC (Fig. 4A,B) ($p < 0.01$). Additionally, Western blot analysis showed that NAC treatment downregulated *c-Myc* expression in hEM15A cells (Fig. 4C; $p < 0.001$). These results indicate the presence of a "ROS/*c-Myc*/*SLC1A5*" pathway in hEM15A cells.

To investigate whether this pathway promotes ferroptosis, hEM15A cells were treated with Erastin, and ROS was neutralized with NAC. Key markers of Gln metabolism and ferroptosis were then evaluated. Significant downregulation of Glu, Gln, Fe^{2+}, and MDA levels were observed, while GSH levels increased (Fig. 4D–H; $p < 0.001$; Fig. 4). Western blot analysis also revealed upregulation of GPX4 expression following ROS clearance (Fig. 4I). These findings further confirm that Erastin enhances the sensitivity of hEM15A cells to ferroptosis via the ROS/*c-Myc*/*SLC1A5* pathway.

3.4 Altered Expression of SLC1A5, c-Myc, and Glutamine in a Rat Model of EMs

HE staining revealed ectopic endometrial tissue in the rat EM model, with glandular structures resembling normal endometrium but displaying an irregular morphology. The glands were surrounded by stromal tissue and displayed fibrotic changes and signs of tissue repair. Extravasation of red blood cells and hemosiderin deposition were also observed. No such pathological changes were observed in the Control group (Fig. 5A), thus confirming the establishment of a rat EMs model. The volume of ectopic EMs lesions was measured using an ultrasound imaging system, and pelvic adhesions were scored according to the Haber scale. The lesion volume in the EMs group was 89.5 mm^3 and the adhesion score was 8.3. This indicates a severe degree of pelvic adhesion, which is a common complication of EMs (Fig. 5B). *SLC1A5* and *c-Myc* expression in the ectopic lesions of the EMs model were significantly lower compared to the Control group (Fig. 5C,D; $p < 0.01$). Furthermore, serum Gln and Glu levels were significantly lower in the EMs lesions (Fig. 5E; $p < 0.01$; Fig. 5). These findings suggest that *SLC1A5* and *c-Myc* are involved in the pathogenesis of EMs.

3.5 Erastin Ameliorates EMs in Rats via the ROS/c-Myc/SLC1A5 Pathway

To investigate the effect of Erastin on rats with EMs, Erastin alone or in combination with NAC was administered intraperitoneally. Ectopic EMs lesions in the Erastin group exhibited structural abnormalities, interstitial porosity, and epithelial cell necrosis (Fig. 6A). The improvement in ectopic lesions in the Erastin+NAC group was less pronounced than in the Erastin alone group. Moreover, the lesion volume and pelvic adhesion score in the Erastin only group (21.2 ± 2.0 mm^3 and 2.7 ± 0.2, respectively) were significantly lower compared to the EMs Model group (94.8 ± 13.5 mm^3 and 8.3 ± 0.6) (Fig. 6B; $p < 0.01$). When NAC was used to clear ROS from the ectopic tissue, the lesion size increased from 21.2 ± 2.0 mm^3 in the Erastin only group to 34.9 ± 2.6 mm^3 in the Erastin+NAC group, while the pelvic adhesion score increased from 2.7 ± 0.2 to 4.3 ± 0.4 ($p < 0.05$).

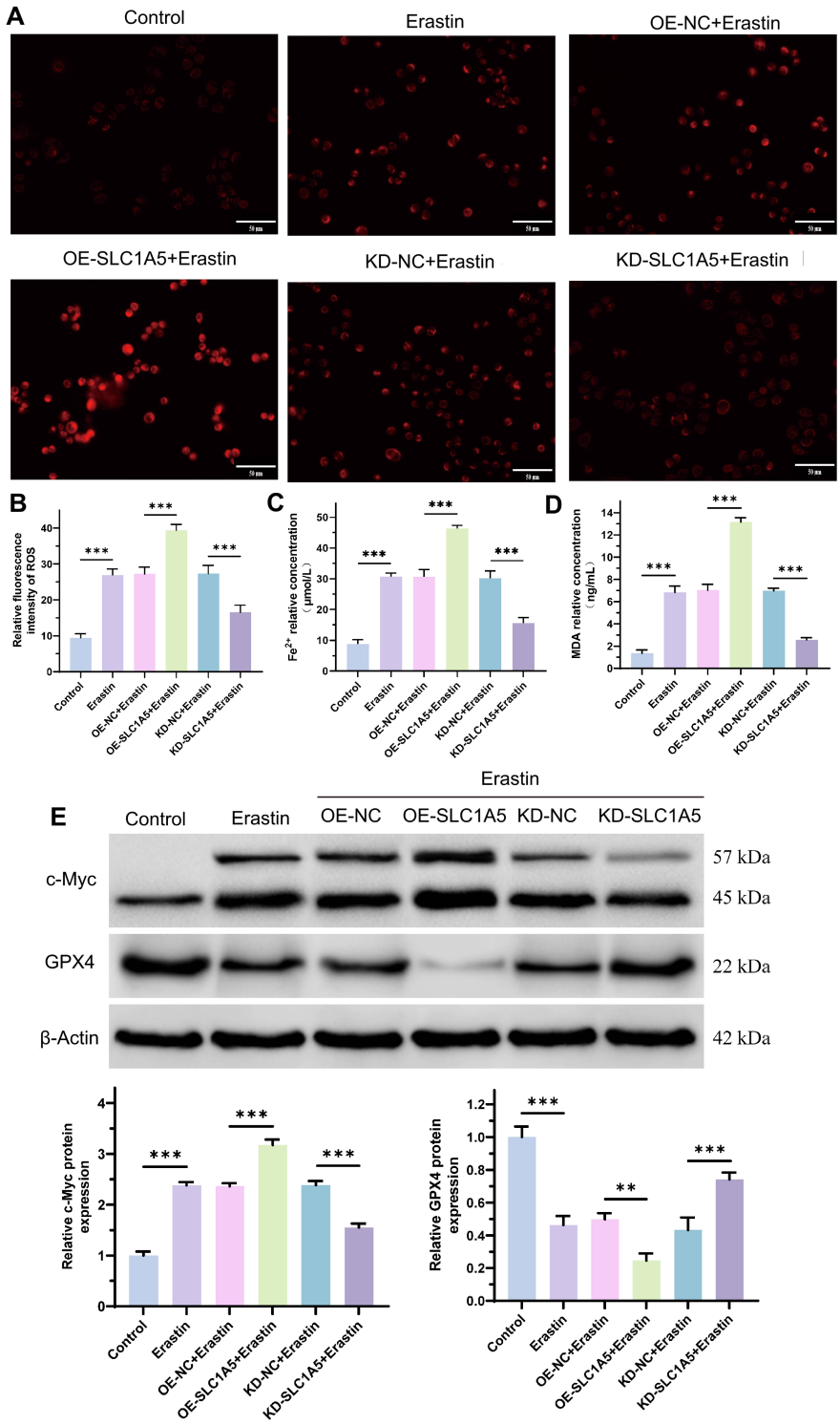

Fig. 3. Oxidative stress markers and protein expression in hEM15A cells under different treatment conditions. (A,B) ROS levels in hEM15A cells with modulated *SLC1A5* expression were assessed using fluorescent probes. No significant differences were observed between the empty vector and Erastin-treated groups, indicating that NC did not alter the mitochondrial ROS level. Scale bar: 50 μm. (C,D) Erastin treatment significantly increased Fe^{2+} and MDA levels in hEM15A cells ($p < 0.001$). Overexpression of *SLC1A5* further increased these levels, whereas *SLC1A5* knockdown reduced them. (E) Western blot and quantitative analysis of *c-Myc* and GPX4 protein levels. Erastin treatment increased *c-Myc* expression and inhibited GPX4 expression in hEM15A cells. *SLC1A5* overexpression significantly increased *c-Myc* ($p < 0.01$) and decreased GPX4 ($p < 0.001$), whereas *SLC1A5* knockdown reduced *c-Myc* and increased GPX4 expression (both $p < 0.01$). $^{**}p < 0.01$, $^{***}p < 0.001$, n = 3.

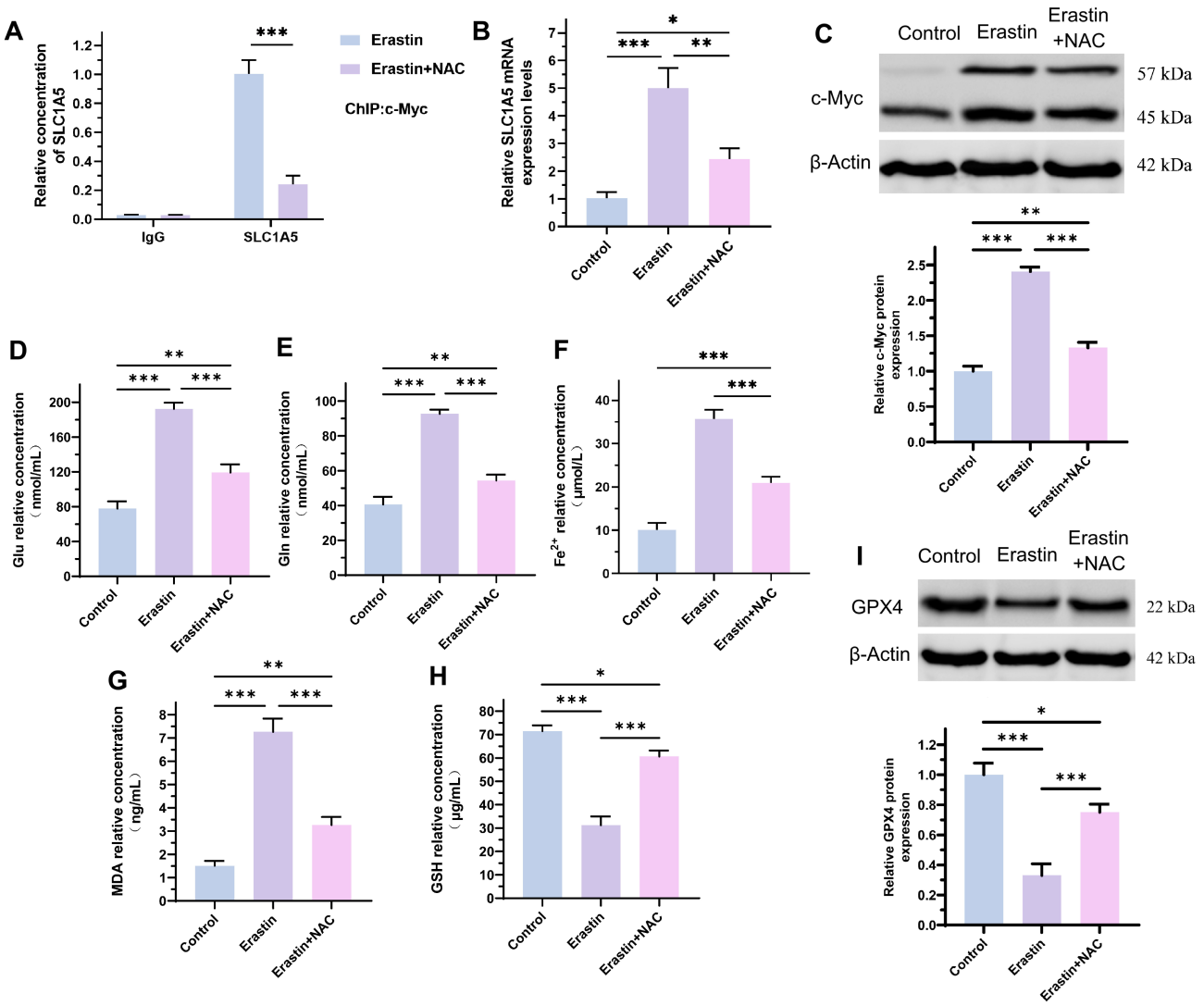

Fig. 4. Regulation of *SLC1A5* expression and its impact on cellular metabolites in Erastin-treated hEM15A cells. (A,B) ChIP analysis showed that *c-Myc* binds to the promoter region of *SLC1A5*, thereby promoting its transcription. Treatment with the ROS scavenger N-acetylcysteine (NAC) reduced ROS levels and suppressed *SLC1A5* mRNA expression ($p < 0.01$). (C) Western blot analysis showed that treatment with NAC downregulated *c-Myc* expression in hEM15A cells ($p < 0.001$). (D–H) Treatment of hEM15A cells with NAC significantly downregulated Glu, Gln, Fe^{2+}, and MDA levels, while upregulating the GSH level ($p < 0.001$). (I) Western blot analysis showed that ROS clearance with NAC resulted in upregulation of GPX4 expression in hEM15A cells. *$p < 0.05$, **$p < 0.01$, ***$p < 0.001$, n = 3.

Fluorescent probes showed that Erastin significantly increased ROS levels in ectopic tissues from the EMs Model compared to the Control group (Fig. 6C). Conversely, the Erastin+NAC group exhibited a substantial decrease in ROS level, indicating that NAC effectively cleared ROS ($p < 0.001$; Fig. 6). The Erastin group displayed notably elevated SLC1A5 and c-Myc mRNA and protein levels compared to the EM Model group (Fig. 6D,E). However, these levels were significantly lower in the Erastin+NAC group compared to the Erastin group ($p < 0.05$; Fig. 6). The Erastin group exhibited significantly higher serum levels of TNF-α, IL-6, and IL-1β than the EMs Model group (Fig. 6F). NAC significantly reduced the levels of these inflammatory factors by eliminating ROS ($p < 0.001$; Fig. 6). The above results suggest that Erastin improves EMs in a rat model by modulating the ROS/*c-Myc*/*SLC1A5* pathway.

4. Discussion

Gln is one of the most plentiful amino acids in humans, playing a crucial role in the tricarboxylic acid cycle and in the synthesis of nucleotides, non-essential amino acids, fatty acids, and ATP [32,33]. In this study, we observed abnormal levels of *SLC1A5*, *c-Myc*, and Gln metabolism in

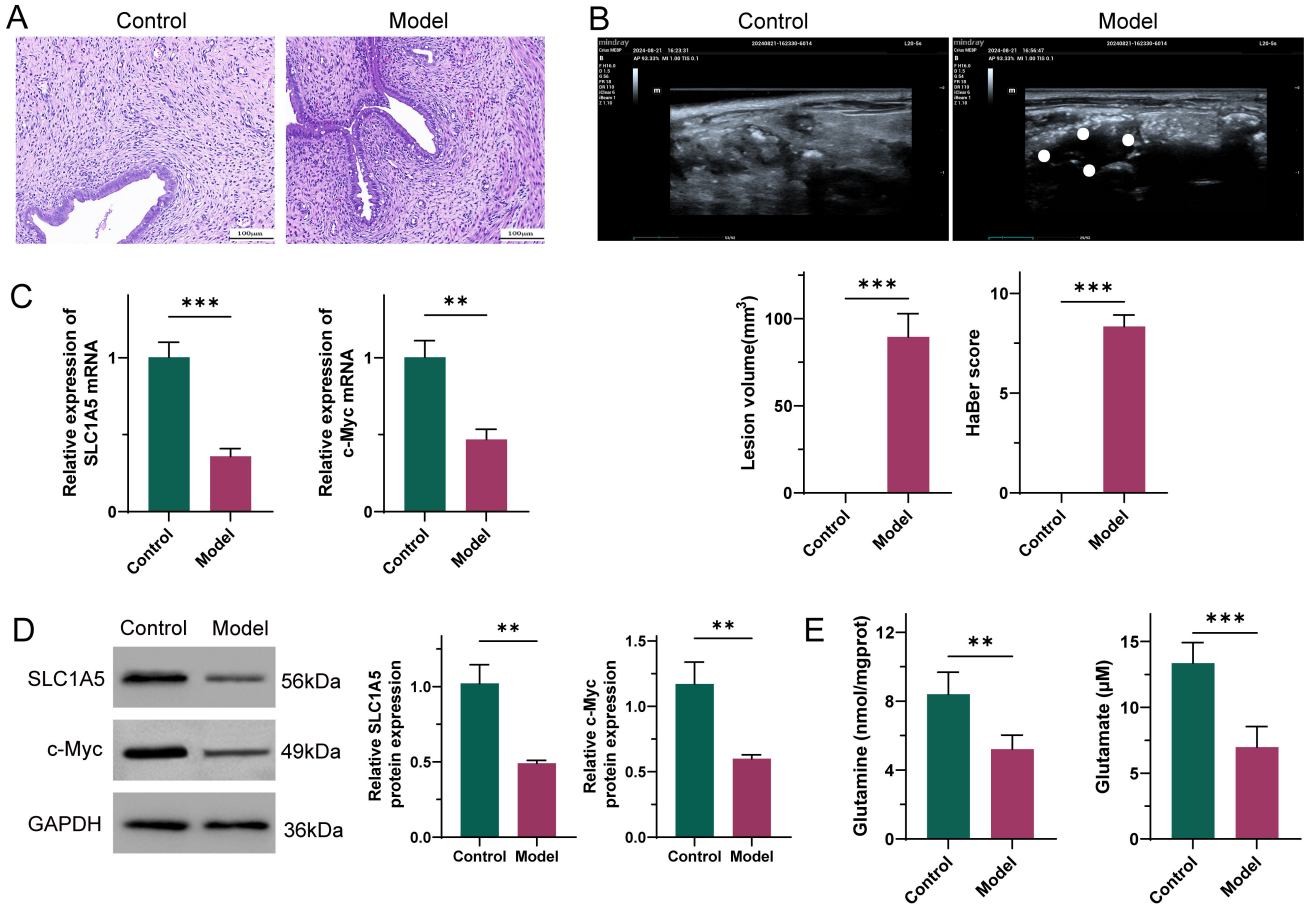

Fig. 5. Histopathological characteristics, lesion volume, adhesion score, and molecular characteristics of a rat endometriosis (EMs) model. (A) Hematoxylin and eosin (HE) staining and pathological changes in ectopic EMs lesions. These revealed disordered heterotopic tissue with signs of repair and fibrosis. No such changes were observed in the Control group, thus confirming successful establishment of the rat EMs model. Scale bar: 100 μm. (B) Ectopic lesion volume and pelvic adhesion were assessed using an ultrasound imaging system, with scoring based on the Haber criteria. The boundaries of the lesions are marked using white dots. The average lesion volume in the EMs group was 89.5 ± 13.3 mm^3 and the average adhesion score was 8.3 ± 0.6, indicating severe pelvic adhesion. This is a common complication of EMs. (C,D) Detection of *SLC1A5* and *c-Myc* expression by RT-qPCR and Western blot. *SLC1A5* and *c-Myc* expression were significantly lower in the EMs group compared to the Control group ($p < 0.01$). (E) Measurement of Gln and Glu levels using an ELISA kit. Serum Gln and Glu levels were significantly lower in the EMs model compared to the Control. $^{**}p < 0.01$, $^{***}p < 0.001$, n = 3.

rats with endometriosis. Moreover, treatment of ESCs with the ferroptosis agonist Erastin significantly upregulated the mRNA level of *SLC1A5*, accompanied by a marked increase in intracellular ROS level. Erastin targets mitochondrial voltage-dependent anion channels (VDAC) to increase mitochondrial outer membrane permeability, leading to active mitochondrial metabolism, reduced glycolysis, and enhanced oxidative stress. This increases ROS generation and lipid damage, eventually triggering ferroptosis of cells [34]. Previous study has demonstrated that Erastin induces iron overload, thereby triggering ferroptosis in ESCs and contributing to the regression of endometriotic lesions. These findings suggest that induction of ferroptosis may offer a potential therapeutic approach for treating EMs [25].

In the present study, Erastin treatment reduced the volume of ectopic lesions and the degree of pelvic adhesion in a rat model of EMs, while also increasing the levels of *SLC1A5*, *c-Myc*, ROS. These effects were significantly reversed when a ROS scavenger was added, confirming the involvement of ROS in the therapeutic effects of Erastin. Furthermore, we found that upregulation of ROS levels by Erastin resulting in ferroptosis of ESCs may be linked to the upregulation of *SLC1A5* expression. The metabolic breakdown of Gln to Glu and α-ketoglutarate in the mitochondria leads to the generation of oxidizable lipids through the tricarboxylic acid cycle, which in turn induces ferroptosis [35]. Additionally, Glu inhibits the system Xc^--dependent cystine uptake pathway, reduces GSH production, and promotes lipid peroxidation to further drive ferroptosis [31].

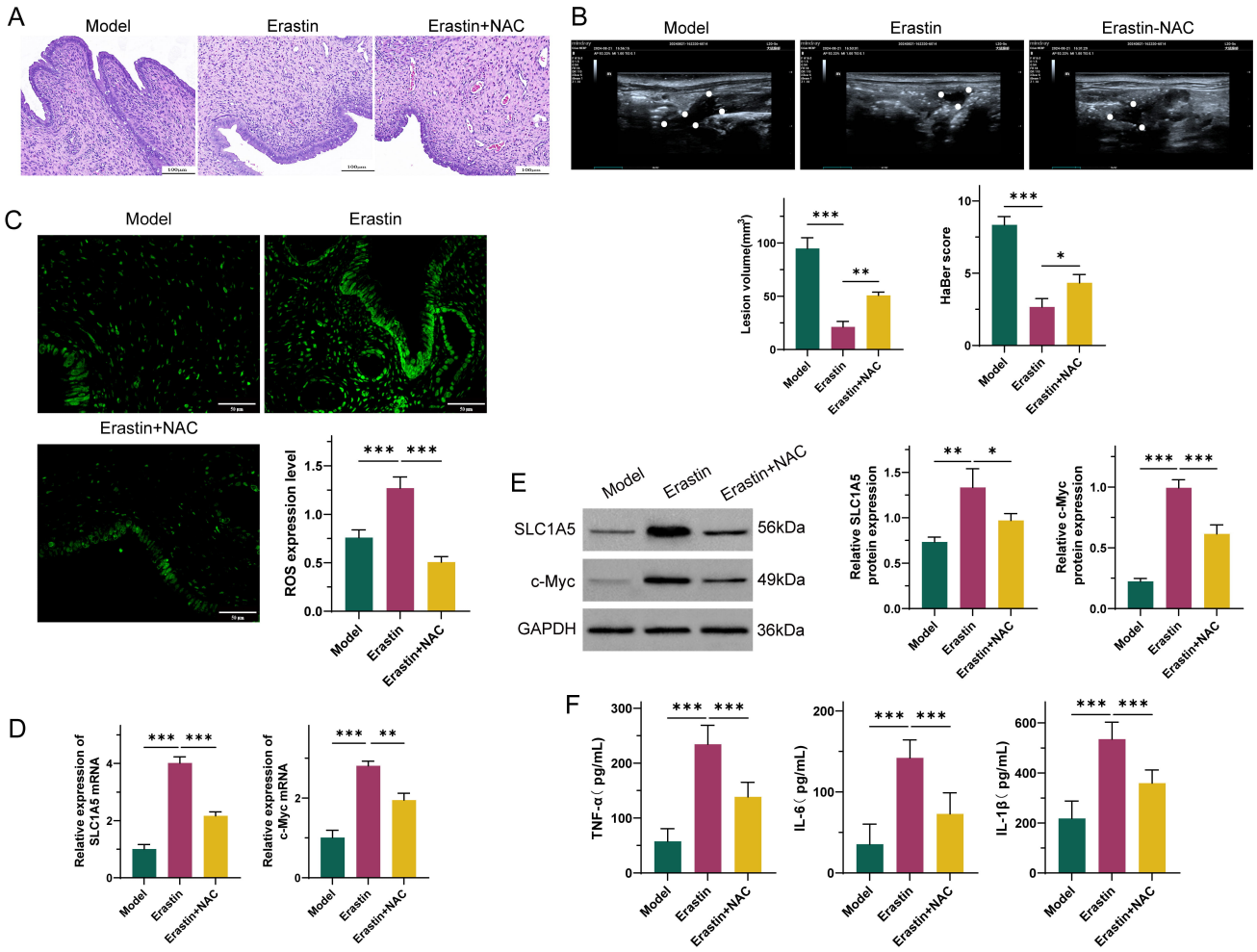

Fig. 6. Evaluation of the therapeutic effect of Erastin in a rat model of EMs, and the effect of ROS. (A) Erastin treatment induced structural abnormalities, interstitial porosity, and epithelial cell necrosis in ectopic EMs lesions. This improvement was less pronounced in the Erastin+NAC group compared to the Erastin group. Scale bar: 100 µm. (B) Ectopic lesion volume and pelvic adhesion were assessed using an ultrasound imaging system, with scoring based on the Haber criteria. The boundaries of the lesions are marked using white dots. The lesion volume and pelvic adhesion score were significantly reduced in the Erastin group compared to the EM Model and Erastin+NAC groups ($p < 0.01$). (C) ROS levels were assessed using a fluorescent probe. Erastin significantly increased ROS levels in ectopic EM lesions compared to the Control group, while the Erastin+NAC group showed a substantial decrease in ROS, indicating effective ROS clearance by NAC ($p < 0.001$). Scale bar: 50 µm. (D,E) *SLC1A5* and *c-Myc* expression were measured by RT-qPCR and Western blot. The Erastin group showed significantly higher mRNA and protein expression of *SLC1A5* and *c-Myc* compared to the EMs Model group, while the Erastin+NAC group exhibited significantly lower levels ($p < 0.05$). (F) Measurement of serum TNF-α, IL-6, and IL-1β levels using an ELISA kit. The Erastin group showed significantly higher levels of TNF-α, IL-6, and IL-1β compared to the EMs Model group, while NAC treatment significantly reduced these inflammatory factors by eliminating ROS ($p < 0.001$). *$p < 0.05$, **$p < 0.01$, ***$p < 0.001$, n = 3.

We investigated the role of *SLC1A5* in Erastin-induced ferroptosis by modulating its expression in ESCs treated with Erastin. Our results showed that Erastin significantly altered the levels of Glu, Gln and GSH in ESCs, as well as the mitochondrial membrane potential, indicating that Erastin promotes *SLC1A5*-mediated Gln metabolism. Furthermore, modulation of *SLC1A5* expression influenced ROS, Fe^{2+}, MDA, *c-Myc*, and GPX4 levels in ESCs, thus providing additional evidence that *SLC1A5* plays a crucial role in ferroptosis. *SLC1A5* is one of the key Gln transporter proteins in mitochondria, and facilitates its entry into cells for subsequent metabolism. The overexpression of *SLC1A5* has been shown to increase cellular sensitivity to ferroptosis [36,37], probably due to its involvement in Gln metabolism. We further confirmed the existence of a ROS/*c-Myc*/*SLC1A5* positive feedback pathway. Removal of ROS in Erastin-treated ESCs caused a reduction in *c-Myc*-mediated *SLC1A5* expression, along with decreased

c-Myc protein expression. The levels of Glu, Gln, Fe^{2+}, MDA, and GSH were also significantly affected by ROS clearance, indicating that Erastin enhances the sensitivity of ESCs to ferroptosis via the ROS/*c-Myc*/*SLC1A5* pathway.

We observed that Erastin treatment in a rat model of EMs reduced the volume of ectopic lesions and pelvic adhesions, while decreasing the levels of SLC1A5, c-Myc, ROS, and inflammatory factors. These therapeutic effects were significantly reversed by NAC. As a GSH precursor, NAC directly counters the inhibition by Erastin of system Xc^- and GSH depletion, while broadly scavenging ROS. This aligns with our experimental design and effectively addresses the multifaceted ROS increase observed in hEM15A cells and in the rat EMs model. The reversal by NAC further supports the critical role of the ROS/c-Myc/SLC1A5 pathway in the progression of EMs. These findings suggest that Erastin may serve as a potential therapeutic agent for managing EMs by modulating SLC1A5 expression and enhancing ferroptosis sensitivity.

Nevertheless, this study has several limitations. A larger sample size for the animal studies, and the use of additional models are needed to further validate the role of Erastin in endometriosis. Future treatment strategies for endometriosis may also involve combining Erastin with therapies that target *SLC1A5*.

5. Conclusion

In conclusion, this is the first study to show that the ROS/c-Myc/SLC1A5 pathway regulates Erastin-induced sensitivity to ferroptosis in endometriosis, thus identifying a novel therapeutic target based on the ferroptosis mechanism. The ability of Erastin to reduce lesion volume through this pathway highlights its potential for the management of EMs, and may be translatable into clinical practice through further drug development and biomarker-guided approaches. However, additional research is required to validate its safety and efficacy in humans, optimize the dosing, and conduct clinical trials to confirm its therapeutic viability.

This study shows SLC1A5 enhances ferroptosis sensitivity in endometriosis. Erastin reduced lesion size and markers in a rat model, but long-term effects and human toxicity (e.g., off-target ferroptosis or metabolic issues) are unstudied. Using only preclinical cells and rats, it lacks human data. Long-term animal studies, pharmacokinetics, and human tissue validation are needed to confirm Erastin's therapeutic potential.

Availability of Data and Materials

All data analyzed during this study are included in this published article. Raw data sets for current study are available from the author (HYM and MXW) upon reasonable request.

Author Contributions

All authors contributed to the study's design and preparation and read and approve the final version of the manuscript. HYM: Experimental execution, data collection and analysis, interpretation of results, writing, and manuscript revision. HYW and JX: Animal experimental design. PYC, BZ, and YHZ: Experimental execution, analysis and interpretation of data. YTX and YYL: Specimen acquisition. MXW: Experimental execution, supervision, review and editing, and funding acquisition. All authors contributed to editorial changes in the manuscript. All authors have participated sufficiently in the work and agreed to be accountable for all aspects of the work.

Ethics Approval and Consent to Participate

The experimental protocols were approved by the Medical Ethics Review Board of The Tenth Affiliated Hospital, Southern Medical University (Dongguan People's Hospital) (Approval No. IACUC-AWEC-202410028). All procedures were conducted in accordance with the Regulations on the Administration of Laboratory Animals (China, 2017) and the ARRIVE Guidelines for the ethical treatment and reporting of animal experiments.

Acknowledgment

The authors sincerely acknowledge the exceptional support and assistance provided by the Central Research Laboratory at The Tenth Affiliated Hospital, Southern Medical University (Dongguan People's Hospital) in conducting this work. We would also like to express our sincere gratitude to members of the mentor group, Dr. Ning Xiaodong and Dr. Chen Peier, for their invaluable guidance and support throughout the experimental process. Their expertise and encouragement have been instrumental in the successful completion of this study.

Funding

This research received no external funding.

Conflict of Interest

The authors declare no conflict of interest.

Supplementary Material

Supplementary material associated with this article can be found, in the online version, at https://doi.org/10.31083/FBL36781.

References

[1] Abramiuk M, Grywalska E, Małkowska P, Sierawska O, Hrynkiewicz R, Niedźwiedzka-Rystwej P. The Role of the Immune System in the Development of Endometriosis. Cells. 2022; 11: 2028. https://doi.org/10.3390/cells11132028.

[2] Koninckx PR, Ussia A, Adamyan L, Wattiez A, Gomel V, Martin DC. Pathogenesis of endometriosis: the genetic/epigenetic

theory. Fertility and Sterility. 2019; 111: 327–340. https://doi.org/10.1016/j.fertnstert.2018.10.013.

[3] Smolarz B, Szyłło K, Romanowicz H. Endometriosis: Epidemiology, Classification, Pathogenesis, Treatment and Genetics (Review of Literature). International Journal of Molecular Sciences. 2021; 22: 10554. https://doi.org/10.3390/ijms221910554.

[4] Wang Y, Wang X, Liao K, Luo B, Luo J. The burden of endometriosis in China from 1990 to 2019. Frontiers in Endocrinology. 2022; 13: 935931. https://doi.org/10.3389/fendo.2022.935931.

[5] Dolmans MM, Donnez J. Emerging Drug Targets for Endometriosis. Biomolecules. 2022; 12: 1654. https://doi.org/10.3390/biom12111654.

[6] França PRDC, Lontra ACP, Fernandes PD. Endometriosis: A Disease with Few Direct Treatment Options. Molecules (Basel, Switzerland). 2022; 27: 4034. https://doi.org/10.3390/molecules27134034.

[7] Diao R, Wei W, Zhao J, Tian F, Cai X, Duan YG. CCL19/CCR7 contributes to the pathogenesis of endometriosis via PI3K/Akt pathway by regulating the proliferation and invasion of ESCs. American Journal of Reproductive Immunology (New York, N.Y.: 1989). 2017; 78. https://doi.org/10.1111/aji.12744.

[8] Shan J, Chang LY, Li DJ, Wang XQ. Rab27b promotes endometriosis by enhancing invasiveness of ESCs and promoting angiogenesis. American Journal of Reproductive Immunology (New York, N.Y.: 1989). 2023; 90: e13762. https://doi.org/10.1111/aji.13762.

[9] Atkins HM, Bharadwaj MS, O'Brien Cox A, Furdui CM, Appt SE, Caudell DL. Endometrium and endometriosis tissue mitochondrial energy metabolism in a nonhuman primate model. Reproductive Biology and Endocrinology: RB&E. 2019; 17: 70. https://doi.org/10.1186/s12958-019-0513-8.

[10] Chen C, Zhou Y, Hu C, Wang Y, Yan Z, Li Z, *et al*. Mitochondria and oxidative stress in ovarian endometriosis. Free Radical Biology & Medicine. 2019; 136: 22–34. https://doi.org/10.1016/j.freeradbiomed.2019.03.027.

[11] Jiang X, Stockwell BR, Conrad M. Ferroptosis: mechanisms, biology and role in disease. Nature Reviews. Molecular Cell Biology. 2021; 22: 266–282. https://doi.org/10.1038/s41580-020-00324-8.

[12] Wu J, Zhang L, Wu S, Liu Z. Ferroptosis: Opportunities and Challenges in Treating Endometrial Cancer. Frontiers in Molecular Biosciences. 2022; 9: 929832. https://doi.org/10.3389/fmolb.2022.929832.

[13] Liu S, Cao X, Zhang T, Zhang C, Qu J, Sun Y, *et al*. Paeonol ameliorates endometrial hyperplasia in mice via inhibiting PI3K/AKT pathway-related ferroptosis. Phytomedicine: International Journal of Phytotherapy and Phytopharmacology. 2023; 109: 154593. https://doi.org/10.1016/j.phymed.2022.154593.

[14] Amaya ML, Inguva A, Pei S, Jones C, Krug A, Ye H, *et al*. The STAT3-MYC axis promotes survival of leukemia stem cells by regulating SLC1A5 and oxidative phosphorylation. Blood. 2022; 139: 584–596. https://doi.org/10.1182/blood.2021013201.

[15] White MA, Lin C, Rajapakshe K, Dong J, Shi Y, Tsouko E, *et al*. Glutamine Transporters Are Targets of Multiple Oncogenic Signaling Pathways in Prostate Cancer. Molecular Cancer Research: MCR. 2017; 15: 1017–1028. https://doi.org/10.1158/1541-7786.MCR-16-0480.

[16] Zhao X, Petrashen AP, Sanders JA, Peterson AL, Sedivy JM. SLC1A5 glutamine transporter is a target of MYC and mediates reduced mTORC1 signaling and increased fatty acid oxidation in long-lived Myc hypomorphic mice. Aging Cell. 2019; 18: e12947. https://doi.org/10.1111/acel.12947.

[17] Anastasi E, Scaramuzzino S, Viscardi MF, Viggiani V, Piccioni MG, Cacciamani L, *et al*. Efficacy of N-Acetylcysteine on Endometriosis-Related Pain, Size Reduction of Ovarian Endometriomas, and Fertility Outcomes. International Journal of Environmental Research and Public Health. 2023; 20: 4686. https://doi.org/10.3390/ijerph20064686.

[18] Mwaura AN, Riaz MA, Maoga JB, Mecha E, Omwandho COA, Scheiner-Bobis G, *et al*. Activin A Modulates Betaglycan Shedding via the ALK4-SMAD3-Dependent Pathway in Endometriotic Cells. Biomolecules. 2022; 12: 1749. https://doi.org/10.3390/biom12121749.

[19] Ruan J, Tian Q, Li S, Zhou X, Sun Q, Wang Y, *et al*. The IL-33-ST2 axis plays a vital role in endometriosis via promoting epithelial-mesenchymal transition by phosphorylating β-catenin. Cell Communication and Signaling: CCS. 2024; 22: 318. https://doi.org/10.1186/s12964-024-01683-x.

[20] Zhan H, Peng B, Ma J, Lin K, Xu K, Lin J, *et al*. Epidermal growth factor promotes stromal cells migration and invasion via up-regulation of hyaluronate synthase 2 and hyaluronan in endometriosis. Fertility and Sterility. 2020; 114: 888–898. https://doi.org/10.1016/j.fertnstert.2020.05.005.

[21] Lu Q, Huang Y, Wu J, Guan Y, Du M, Wang F, *et al*. T-cadherin inhibits invasion and migration of endometrial stromal cells in endometriosis. Human Reproduction (Oxford, England). 2020; 35: 145–156. https://doi.org/10.1093/humrep/dez252.

[22] Marcellin L, Santulli P, Chouzenoux S, Cerles O, Nicco C, Dousset B, *et al*. Alteration of Nrf2 and Glutamate Cysteine Ligase expression contribute to lesions growth and fibrogenesis in ectopic endometriosis. Free Radical Biology & Medicine. 2017; 110: 1–10. https://doi.org/10.1016/j.freeradbiomed.2017.04.362.

[23] Wang H, Wang B, Wu M, Lu J, Duan P. Targeting osteopontin alleviates endometriosis and inflammation by inhibiting the RhoA/ROS axis and achieves non-invasive in vitro detection via menstrual blood. Human Reproduction (Oxford, England). 2024; 39: 1057–1071. https://doi.org/10.1093/humrep/deae052.

[24] Abe W, Nasu K, Nakada C, Kawano Y, Moriyama M, Narahara H. miR-196b targets c-myc and Bcl-2 expression, inhibits proliferation and induces apoptosis in endometriotic stromal cells. Human Reproduction (Oxford, England). 2013; 28: 750–761. https://doi.org/10.1093/humrep/des446.

[25] Li Y, Zeng X, Lu D, Yin M, Shan M, Gao Y. Erastin induces ferroptosis via ferroportin-mediated iron accumulation in endometriosis. Human Reproduction (Oxford, England). 2021; 36: 951–964. https://doi.org/10.1093/humrep/deaa363.

[26] Bashir ST, Redden CR, Raj K, Arcanjo RB, Stasiak S, Li Q, *et al*. Endometriosis leads to central nervous system-wide glial activation in a mouse model of endometriosis. Journal of Neuroinflammation. 2023; 20: 59. https://doi.org/10.1186/s12974-023-02713-0.

[27] Zhang Y, He T, Lin T, Guo Q, Huo C, Roberts SZ, *et al*. Novel in vivo endometriotic models associated eutopic endometrium by implanting menstrual blood-derived stromal cells from patients with endometriosis. Scientific Reports. 2023; 13: 8347. https://doi.org/10.1038/s41598-023-35373-4.

[28] Assaf L, Eid AA, Nassif J. Role of AMPK/mTOR, mitochondria, and ROS in the pathogenesis of endometriosis. Life Sciences. 2022; 306: 120805. https://doi.org/10.1016/j.lfs.2022.120805.

[29] D'Amico R, Impellizzeri D, Cordaro M, Siracusa R, Interdonato L, Marino Y, *et al*. Complex Interplay between Autophagy and Oxidative Stress in the Development of Endometriosis. Antioxidants (Basel, Switzerland). 2022; 11: 2484. https://doi.org/10.3390/antiox11122484.

[30] Wu K, Gong W, Hu JC, Duan YC, Ke HH, Chen L. SLC38A2 promotes cell proliferation and invasion by promoting glutamine metabolism in adenomyosis. Experimental and Therapeutic Medicine. 2024; 27: 218. https://doi.org/10.3892/etm.

2024.12506.
[31] Dixon SJ, Lemberg KM, Lamprecht MR, Skouta R, Zaitsev EM, Gleason CE, *et al*. Ferroptosis: an iron-dependent form of nonapoptotic cell death. Cell. 2012; 149: 1060–1072. https://doi.org/10.1016/j.cell.2012.03.042.
[32] Gandasi NR, Arapi V, Mickael ME, Belekar PA, Granlund L, Kothegala L, *et al*. Glutamine Uptake via SNAT6 and Caveolin Regulates Glutamine-Glutamate Cycle. International Journal of Molecular Sciences. 2021; 22: 1167. https://doi.org/10.3390/ijms22031167.
[33] Yoo HC, Yu YC, Sung Y, Han JM. Glutamine reliance in cell metabolism. Experimental & Molecular Medicine. 2020; 52: 1496–1516. https://doi.org/10.1038/s12276-020-00504-8.
[34] Zhao Y, Li Y, Zhang R, Wang F, Wang T, Jiao Y. The Role of Erastin in Ferroptosis and Its Prospects in Cancer Therapy. OncoTargets and Therapy. 2020; 13: 5429–5441. https://doi.org/10.2147/OTT.S254995.
[35] Rodríguez-Graciani KM, Chapa-Dubocq XR, Ayala-Arroyo EJ, Chaves-Negrón I, Jang S, Chorna N, *et al*. Effects of Ferroptosis on the Metabolome in Cardiac Cells: The Role of Glutaminolysis. Antioxidants (Basel, Switzerland). 2022; 11: 278. https://doi.org/10.3390/antiox11020278.
[36] Han L, Zhou J, Li L, Wu X, Shi Y, Cui W, *et al*. SLC1A5 enhances malignant phenotypes through modulating ferroptosis status and immune microenvironment in glioma. Cell Death & Disease. 2022; 13: 1071. https://doi.org/10.1038/s41419-022-05526-w.
[37] Xu F, Wang H, Pei H, Zhang Z, Liu L, Tang L, *et al*. SLC1A5 Prefers to Play as an Accomplice Rather Than an Opponent in Pancreatic Adenocarcinoma. Frontiers in Cell and Developmental Biology. 2022; 10: 800925. https://doi.org/10.3389/fcell.2022.800925.